Design, Analysis and Related Applications of Shunt Varactor Loaded Reconfigurable Metamaterial Transmission Lines

Omar F. Siddiqui, Ashraf S. Mohra*, and Majeed A. Alkanhal

Department of Electrical Engineering, King Saud University
P.o Box 800, Riyadh 11421, Saudi Arabia
Tel: 966-1-467-75616 Fax: 966-1-467-6757; E-mail: amohra@ksu.edu.sa

***Abstract*- The paper outlines theory and practical applications of shunt varactor loaded metamaterial lines. The traditional metamaterial line is loaded with an additional shunt varactor to get tunable band-pass characteristics. Design equations are developed to synthesize a generalized metamaterial line with arbitrary impedance, phase, and band-pass response characteristics. To illustrate the concept, two compact reconfigurable microwave devices including a Wilkinson power divider with a tunable band-pass response and a tunable phase shifter were designed and fabricated.**

***Index Terms*- Left handed transmission line, Varactors, Tunable Power divider, tunable phase shifter.**

I. INTRODUCTION

The theoretical foundation of metamaterials (MTMs) was laid down by Viktor Vesalago in 1967 when he investigated the possibility of a negative-refractive-index [1]. However, the concept of negative refraction was experimentally demonstrated in 2001 in the synthesized periodic structures that consist of highly resonant split rings and thin metallic wires [2]. Since then, numerous research papers have been published on MTMs (for example see the books [3], [4] and the review paper by Ramakrishna [5] and the references therein). Initially, the term 'metamaterial' was applied to negative-index materials, Later, with the implementation of negative refraction concept in other technologies such as loaded transmission line structures [6] and photonic crystals [7], the scope of application of the term 'metamaterial' has been widened to include all the artificially synthesized periodic structures that demonstrate unusual dispersion characteristics.

The negative-refractive-index (NRI) is the direct consequence of the backward wave propagation that takes place in the lowest harmonic of these periodic structures. As a result, the electric field ***E***, the magnetic field ***H***, and the propagation vector ***k*** form a left-handed triplet, in contrast to normal (right-handed) media. Therefore, these materials have also been termed as "left-handed" media [3]. The transmission-line metamaterials (TL-MTM) are based on the equivalent circuit of the split-ring and thin-wire metamaterial [8]. Hence two dimension (2D) and three dimension (3D) versions of the TL-metamaterials also demonstrate sub-diffraction focusing properties [9, 10]. On the other hand, one dimension (1D) versions of the TL-MTMs have been successfully employed to build compact microwave devices such as phase-shifters, power dividers, filters, and antennas [11-15]. Traditionally, the left-handed MTM lines have been fabricated by loading a host transmission line with series capacitance and shunt inductance. The unit cell of such a loaded transmission line is shown in Fig.1a. These MTM lines exhibit an inherent high-pass backward-wave response in their lowest harmonics, leading to novel microwave devices that are compact and wide-band in nature [11-15].

Earlier reported reconfigurable metamaterial devices, such as the scannable leaky-wave antenna [4] and the phase shifter employ the

tuning of the phase characteristics. On the other hand, this paper deals with controlling the band-pass amplitude characteristics of the metamaterial by the extra shunt varactor loading (C_{sh}), as shown in Fig 1a.

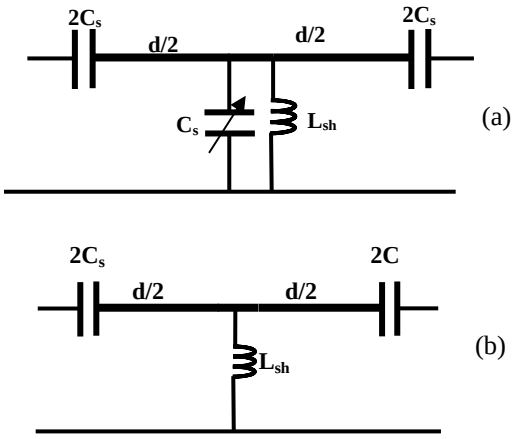

Fig.1 Unit cell of a left-handed metamaterial transmission-line (a) the traditional approach. (b) With an added shunt capacitive loading.

The additional capacitive loading renders more freedom in controlling the cut-off frequency of the fundamental mode and the subsequent stop-band. Consequently, MTM design with a *controllable* band-pass response can be achieved. These MTM lines can thus be utilized in situations where band-suppression is required around the frequency of interest. Furthermore, varactors can be employed to tune the amplitude and phase response of the MTM line resulting in reconfigurable compact devices. In the absence of the shunt capacitor, the length of the MTM line would have to be increased to achieve the required band-pass response.

In the next sections, the dispersion properties of the capacitor-loaded left handed lines are clarified by means of Brillouin diagram**.** Design equations for a MTM TL with arbitrary phase, impedance, and band-pass characteristics are presented. These equations are then applied to design a compact reconfigurable Wilkinson power divider and a compact tunable phase shifter. The practical tunable ranges of these devices depend on the variable capacitance of the varactor. As the demonstration of the concept using available varactor diodes (SMTD 3006-SOD 323), a tunable range of 160 MHz is obtained around the center frequency (800 MHz) of the power divider and a compactness factor of 12 is achieved compared to the conventional power divider. The phase shifter, on the other hand, demonstrates a 100 degree differential phase at a center frequency of 505 MHz. It may be noted that the proposed N-stage shunt-varactor-loaded metamaterial employs least number of varactors (N) to achieve tunable response. On the other hand, the series varactor scheme [16] and series/shunt configuration of the tunable leaky wave antenna [4] employ 2N and 3N varactors respectively to maintain symmetry and balanced dc-bias currents.

II DISPERSION ANALYSIS

Consider the unit cell of the MTM line with periodicity *d*, as depicted in Fig. 1b. The host transmission line has a characteristic impedance of Z_o (admittance $Y_o = 1/Z_o$) and a phase velocity of *u*. Thus the distributed inductance L_o and the capacitance C_o of the unloaded transmission line can be written as:

$$L_o = \frac{Z_o}{u}, \quad C_o = \frac{1}{Z_o u} \tag{1}$$

Assuming the loaded line of Fig 1 extends to infinity, the following dispersion relation is obtained by using the Bloch-Floquet theorem [17]:

$$\cosh \gamma d = \cos \beta d\left[1+\frac{YZ}{4}\right]+ \frac{j}{2}\sin \beta d\left[ZY_o + YZ_o\right]+\frac{YZ}{4} \tag{2}$$

Where the complex Bloch propagation constant γ is composed of the real attenuation constant α and the imaginary phase constant *k* ($\gamma = \alpha + jk$). $\beta = \omega\sqrt{L_o C_o}$ is the intrinsic phase constant of the unloaded line (ω is the radian frequency). Y and

Z are the series admittance and shunt impedance of the loading elements, given by:

$$Y = \frac{1}{j\omega L_{sh}} + j\omega C_{sh} \ , \quad Z = \frac{1}{j\omega C_s} \qquad (3)$$

A simplified version of Eq.(2), which gives more insight into the resonance behavior of the structure can be obtained by assuming the intrinsic and Bloch phase shifts per unit cells to be much less than unity (βd and kd<<1) [8]:

$$kd = \omega\sqrt{L_o dC'}\left[\left(1-\frac{1}{\omega^2 L_o dC_s}\right)\left(1-\frac{1}{\omega^2 L_{sh}C'}\right)\right] \qquad (4)$$

Where $C'=C_o d+C_{sh}$. Under the above assumption, the equivalent circuit can be modified to the one given in Fig.2 in which the distributed inductance and capacitance, contained in the length *d*, are modeled as lumped elements $L_o d$ and $C_o d$. As a representative example, consider the case when the loading elements have the values L_{sh}=6.8nH, Cs=5.6pF, and C_{sh}=8pF and the parameters of the unloaded transmission line are Z_o = 70Ω and u = $3x10^8$. The resulting Brillouin diagram shows the first two harmonic bands of the periodic structure and the impedance states of the series and shunt branches of the unit cell, Fig.3. As a general rule, the structure exhibits a pass-band whenever the shunt and the series branches have opposite reactances i.e. if one is inductive the second should be capacitive for transmission and vice versa [8]. Below the Bragg's frequency f_o, there is a complete cut-off in transmission as the series impedance is very high (open circuit). The Bragg's frequency is given by [8]:

$$f_o = \frac{1}{4\pi\sqrt{L_{sh}C_s}} \qquad (5)$$

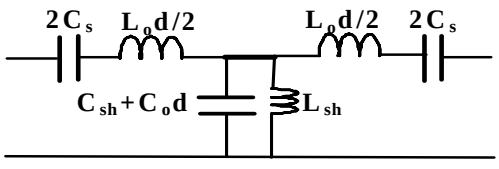

Fig. 2 Equivalent circuit of the unit cell under the assumption kd and βd << 1.

Above the Bragg's frequency, the propagation takes place as a backward wave or in the left-handed mode because the series and shunt branches are capacitive and inductive respectively. This is the fundamental band of the periodic structure. The start and end points of the band-gap (f_L, f_H) depend on which of the two branches (series or shunt) resonates first. The resonant frequencies of the series and shunt resonators, given by:

$$f_s = \frac{1}{2\pi\sqrt{L_o dC_s}} \ , \quad f_{sh} = \frac{1}{2\pi\sqrt{L_{sh}(C_o d + C_{sh})}} \qquad (6)$$

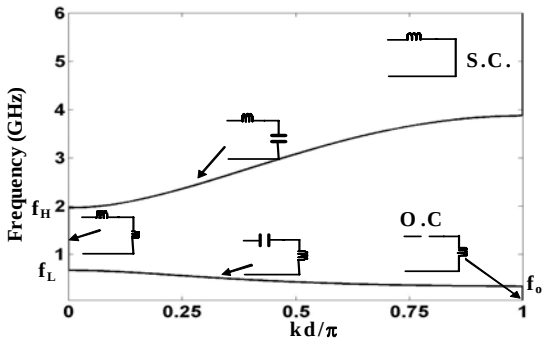

Fig.3 Brillouin Diagram of the capacitor loaded LHTL and the impedance behavior of the shunt and series branches. (O.C. = open circuit and S.C = short circuit).

If C_{sh} is sufficiently large such that $f_{sh} < f_s$, the shunt branch resonates first, signifying the end of the fundamental band and start of the stop-band. In this case $f_L=f_{sh}$ and $f_H=f_s$. Both the series and the shunt branches of the unit cell become inductive above f_L, as shown in Fig.3, causing the stop-band. At f_H, the series branch resonates identifying the start of the second pass-band. As the frequency increases above f_H, the shunt branch becomes capacitive rendering the forward wave pass-band. For very high frequencies, the shunt capacitor C_{sh} is shorted out and the structure is in cut-off. On the other hand, the series branch resonates earlier than the shunt branch for small values of the shunt capacitive loading. In this case the cut-off frequency of the first pass-band becomes $f_L=fs$ and the width of the stop-band is given by $f_s<f<f_{sh}$. As a consequence of these dispersion characteristics,

the fundamental band can be tuned by means of the shunt loading C_{sh} when $f_{sh}<f_s$. The effect of shunt capacitance variation on the resonance frequencies of the structure is graphically displayed in Fig.4. To further illustrate the dependence of C_{sh} on the dispersion characteristics, Brillouin diagrams are drawn for four values of shunt capacitances i.e. 12 pF, 8 pF, 4 pF, and 0.1 pF (Fig.5). Adjacent to the Brillouin diagram, the transmission coefficient (S_{21}) of a terminated two-stage metamaterial line is plotted to show the band pass amplitude characteristics. For high values of C_{sh} (>>C_od), f_H=fs and the cut-off frequency of the fundamental band f_L depends inversely on C_{sh} (Fig.4). As a result, the transmission takes place in the region that extends from f_o to $f_L=f_{sh}$ (see Fig.5). The pass-bands widens as the capacitance is decreased from 12pF to lower values. When C_{sh} becomes considerably small such that f_{sh} becomes larger than fs, f_H starts varying with the shunt capacitance and f_L remains constant at the series resonance f_s.

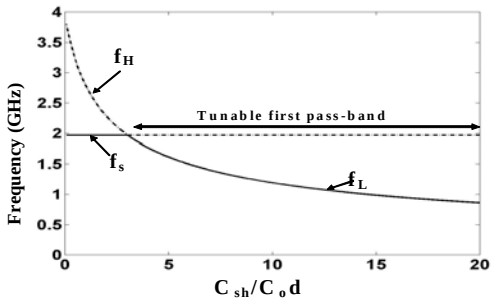

Fig.4 Effect of the value of shunt loading capacitors on the resonances of the periodic structure.

As an example, consider the Brillouin diagram and associated S_{21} plot (Fig. 5d) for C_{sh} = 0.1 pF. The fundamental band has attained its maximum range ($f_o<f<f_s$) extending from 0.4 GHz to 2 GHz. As $C_{sh} \rightarrow 0$, f_H approaches $1/2\pi\sqrt{L_{sh}C_o d}$ and the dispersion becomes similar to that of a left-handed MTM line without a shunt loading [8]. To observe the matching characteristics of the metamaterial, the reflection coefficient (S_{11}) and the Bloch impedance are plotted for different values of shunt loading in Fig. 6. The S_{11} plot shows good matching as the center frequency is varied from 0.4 GHz at 16pF to 0.6 GHz 8 pF (which is about ±20% range about the center). As depicted in Fig. 6b, a small change of ±10Ω from the center value of 70 Ω is noted in this range.

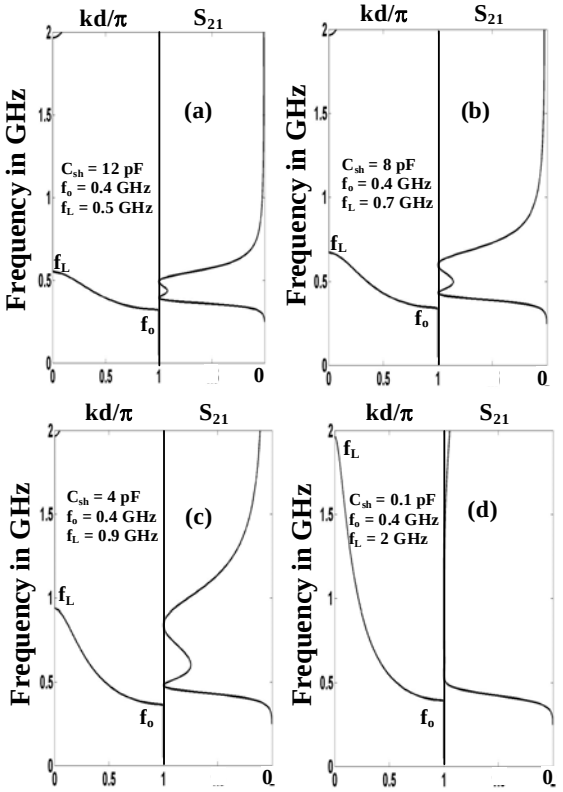

Fig.5 Brillouin diagram and associated transmission coefficient of a terminated capacitor-loaded MTM line showing the effect of shunt capacitive loading.

III. DESIGN EQUATIONS

The objective of the design is to obtain the values of the loading elements (C_s, L_{sh} and C_{sh}) and the periodicity (unit cell length d) for a given MTM transmission line with Bloch impedance Z_B and the unit cell phase shift θ. The other parameters that contribute to the band-pass characteristics are the center operating frequency of the MTM line (f_{center}), the pass-band (f_o, f_L) and the highest frequency of the rejection band (f_H). These frequencies are summarized as follows:

$$\omega_o = \frac{1}{2\sqrt{L_{sh}C_s}}, \quad \omega_L = \frac{1}{\sqrt{L_{sh}C'}},$$
$$\omega_H = \frac{1}{\sqrt{L_o dC_s}}, \ \omega_{center} = (\omega_o + \omega_L)/2 \qquad (7)$$

The phase shift per unit cell (Eq.4) can be further simplified in the fundamental band to the following equation:

$$\theta^2 = (kd)^2 = \frac{1-\omega^2/\omega_L^2}{\omega^2 L_{sh}C_s} \qquad (8)$$

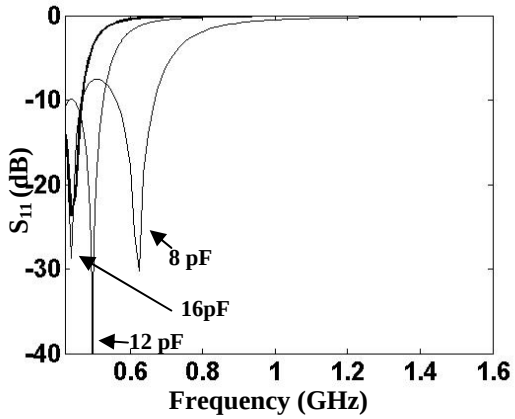

(a)

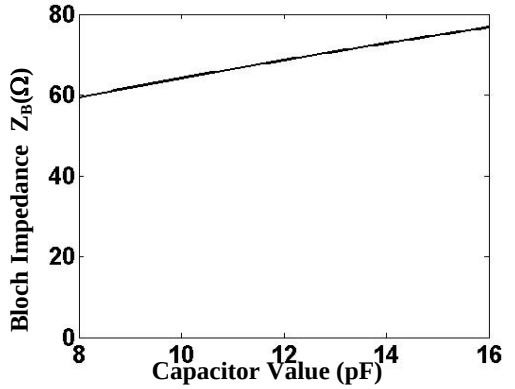

(b)

Fig.6 Matching Characteristics (a) Reflection coefficient (S_{11}) for three shunt capacitive loadings (Csh). (b) Bloch impedance of the metamaterial for the range of shunt loadings 8pF-16pF

Similarly, the Bloch impedance of the periodic structure in the lowest pass-band can be approximated as:

$$Z_B \approx \sqrt{\frac{Z_s}{Y_{sh}}} \qquad (9)$$

Where Z_s and Y_{sh} are the series impedance and shunt admittance of the unit cell of Fig. 2. Inserting these values in (Eq.8) and after some algebraic manipulations, following relation of the Bloch impedance is obtained:

$$Z_B^2 = \frac{L_{sh}}{C_s}\frac{1-\omega^2/\omega_H^2}{1-\omega^2/\omega_L^2} \qquad (10)$$

Solving (Eq.8) and (Eq.10) at the center frequency, the series capacitance C_s is given by:

$$C_s = \frac{1}{\theta Z_B \omega_{center}}\sqrt{1-\frac{\omega_{center}^2}{\omega_H^2}} \qquad (11)$$

By solving (Eq.11) and the resonance relations given in (Eq.7), the other unknown parameters are then evaluated as follows:

$$d = \frac{1}{L_o C_s \omega_H^2} \qquad (12)$$
$$L_{sh} = \frac{1}{4C_s\omega_o^2} \qquad (13)$$
$$C' = \frac{1}{L_{sh}\omega_L^2} \qquad (14)$$
$$C_{sh} = C' - C_o d \qquad (15)$$

IV. APPLICATIONS

A. The Tunable Power Divider

One of the simplest and most commonly used power dividers is the equal-split Wilkinson's power divider which consists of two λ/4 branches of impedance $\sqrt{2}Z_o$, where Z_o is the impedance of the transmission line system. The dispersion properties of the MTMs have been used to build compact power dividers that demonstrated single band or dual band operation [14], [18-19]. Other techniques have also been applied to build compact and multi-band power divider, such as using Π-shaped sections, [20] and sections of

transmission lines with different electrical lengths [21]. Here we present the design of a power divider with band-pass characteristics by exploiting the dispersion characteristics of the capacitor-loaded MTM lines. Consider a power divider with f_{center} = 0.475 GHz, f_L = 0.4 GHz, and f_H = 1.96 GHz. Using equations (11)-(15) the design parameters are given by C_s = 5.6 pF, L_{sh} = 6.8 nH, C_{sh} = 12 pF, and d = 0.5 cm. To demonstrate the power division, the capacitor-loaded MTM lines are implemented in Agilent's Advanced Design System (ADS) using ideal components. The transmission coefficient (S_{21}) and isolation (S_{32}), plotted in Fig. 7a, show good agreement with the design. The simulated power-divider offers 3dB transmission in the pass-band and about 30 dB as isolation between the output ports. In addition to the isolation, it also provides a good rejection of the adjacent frequencies. The pass-band and stop-band cut-off frequencies also match with the designed values calculate from the equations (11)-(15) and the Brillouin diagram of Fig.5. Simulation results for a shunt capacitor loading of 8 pF, given in Fig.7(b), show that the pass-band extends to 0.67 GHz and the center frequency increases to 0.53 GHz. The transmission and isolation are 3dB and 20dB, respectively. The reflection coefficient for the two shunt loading, given in Fig.8, shows acceptable reflection losses. To verify the simulation results presented above, a MTM-based Wilkinsin power divider is fabricated in microstrip technology. Fig.9 shows schematic of one of the λ/4 branches that is composed of two unit cells. To provide a dc block to the shunt inductor, the single shunt capacitor is replaced by a combination of a fixed capacitor of C_f (24) pF in series with a varactor SMTD3006 (Aeroflex-Metallics) which has a capacitance in the range 7-16pF for a voltage change of 15-1.5V. Therefore, the achievable tunable range of the shunt capacitor (C_{sh}) is between 5.419 pF and 9.6 pF. The fabricated circuit, shown in Fig. 10, is implemented on RT/Duroid 5880 substrate (ε_r=2.2, H=0.7874mm). The overall circuit dimension is 2cm x 2cm which is about 1/20 of the free space wave-length at the center frequency. Alternatively, about twelve times size reduction is obtained compared to a conventional Wilkinson power divider printed on the same substrate.

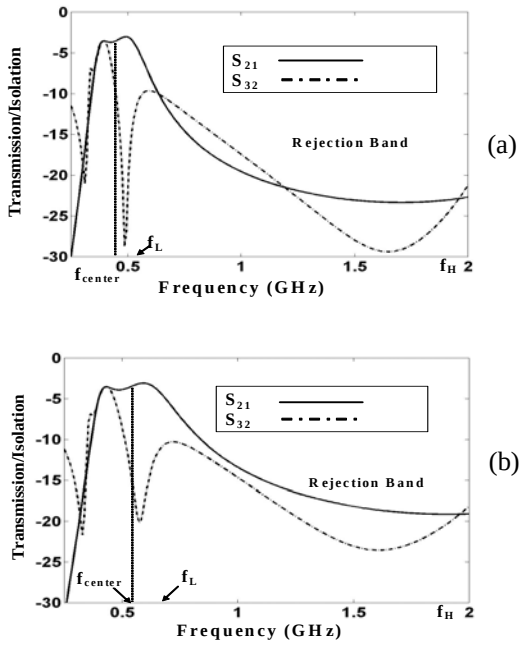

Fig.7 Simulation results of a MTM-based Wilkinson Power Divider with band pass characteristic s with shunt loading C_{sh} equal to (a)12 PF and (b) 8 PF.

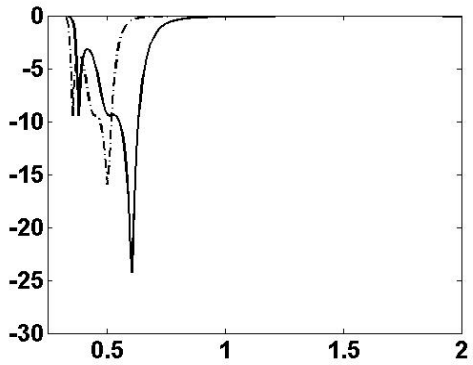

Fig.8 Reflection coefficient of the power divider for the two shunt capacitor loading showing good matching.

The S-parameters were measured by an Anritsu 37369C vector network analyzer. The transmission coefficient S_{21} and the isolation between the output ports are depicted for two voltage-states 4.5 V and 14 volts are shown in

Fig 11. These voltages correspond to a total shunt capacitance of 8 pF and 5.63 pF respectively. As observed in Fig 11a, the overall shape of the band-pass response is similar to the simulations. The pass-band transmission and isolation are given by -4.5dB and -17 dB respectively at a center frequency of 0.725 GHz. There is an excellent rejection of the out-of-band frequencies. Comparing Figs. 7a and 11a, there is a frequency shift of 0.19 GHz between ideal simulations and experiments which is mainly attributed to the varactor capacitance which may vary under different biasing conditions. Other factors are lumped element tolerances, fabrication impurities, and slight shifts in dielectric constant of the substrate.

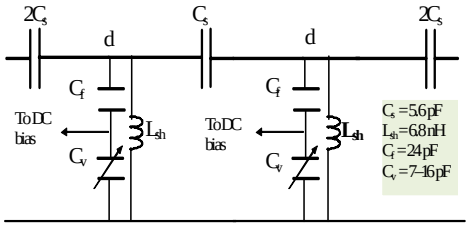

Fig. 9 Single λ/4 branch of the MTM power divider.

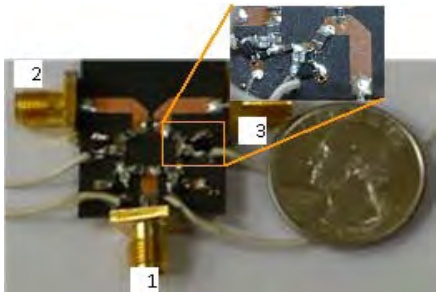

Fig.10 Microstrip implementation of a MTM-based Wilkinson power divider.

For lower value of capacitance (DC bias 14V), the center frequency moves 0.88 GHz and the pass-band widens. The transmission coefficient at the center frequency is about -4.4 dB and an isolation of about -13 dB. To demonstrate the tunability of the power divider, a superposition of scattering parameters determined with varactor voltage-states from 4V to 14 V is depicted in Fig. 12. The transmission in all the cases is better than -4.6 dB and isolation is better than 12 dB. The 22 lumped elements that are used in the RF circuitry are the cause of most of the losses that are introduced into the circuit. The practical reflection loss is better than 11 dB for the whole range, as depicted in Fig. 13.

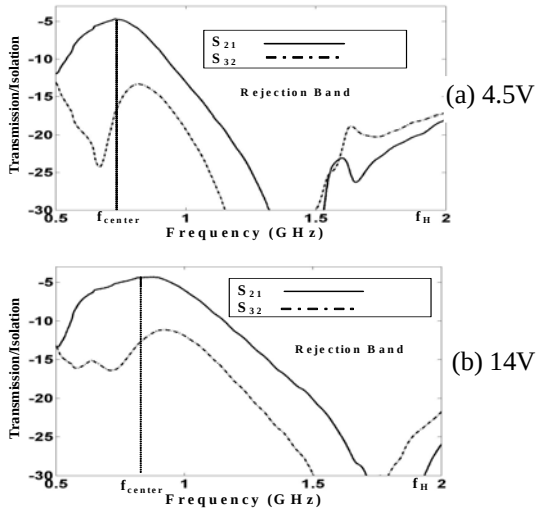

Fig.11 Experimental results for the MTM Wilkinson power divider for two voltage states of the loaded shunt varactor.

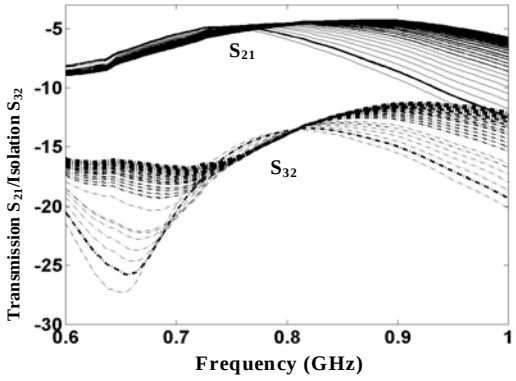

Fig 12 Superposition of S-parameters resulting from shunt varactor voltage states from 4 V to 14 V.

B. The Tunable Phase Shifter

MTM transmission lines have been used previously to build compact passive phase

shifters with static phase response [12] and active shifters with tunable response [16]. The N-stage phase shifters of [16] employ 2N series varactors (two per stage) to distribute balanced dc biasing currents to individual varactors. The N-stage shunt-capacitor loaded metamaterial lines, on the other hand, require only one varactor per cell (a total of N varactors). Consider a 3-stage 50Ω shunt-capacitor loaded MTM with the cut-off frequencies given by f_O = 0.45 GHz and f_H = 2 GHz. The design equations (11)-(15) give L_{sh} = 4.7 nH, C_s = 6.8 pF, and d = 0.5 cm. The MTM line, depicted in Fig. 14, is implemented on a Rogers RT/Duroid 5880 substrate (ε_r=2.2, h=0.7874mm).

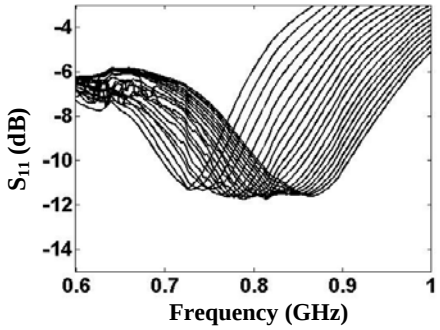

Fig.13 The reflection coefficients of the tunable power divider for all the voltage state.

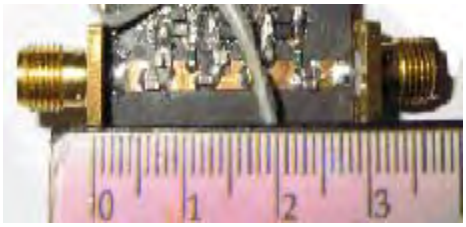

Fig. 14 Fabricated MTM transmission line tunable phase shifter without the biasing network.

To provide a dc block to the shunt inductor and to obtain a reasonable tuning range, the single shunt capacitor is replaced by a combination of a 24pF fixed capacitor in series with two parallel SMTD3006 (Aeroflex-Metallics) varactors that have a capacitance of 7-16 pF with 15-1.5V bias. Hence the tunable range of the shunt capacitor (C_{sh}) is 8.84-14pF. The superimposed experimental S_{21} magnitude and phase and S_{11} magnitude are depicted in Figs. 15-16 for the voltage states 2-15V in the 10% bandwidth region around the center frequency of 505 MHz. A phase change of about 100 degrees is noted when the voltage is varied from 2V to 15V with the magnitude better than -4dB for all the states (better than -3dB for voltage states >4V). The reflection loss is better than 15 dB (Fig. 16) for all the cases. The overall size of the fabricated circuit is about 3cm x 0.5 cm excluding the biasing network. Thus the length is about 1/20 of the free-space wavelength at the center frequency.

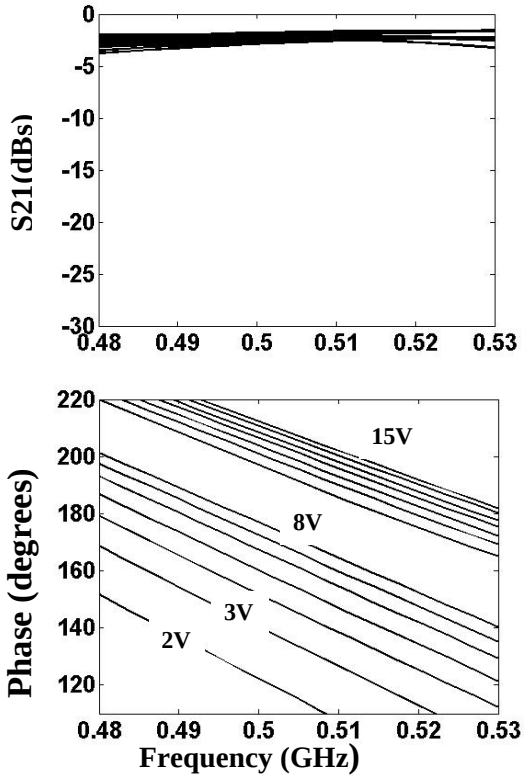

Fig.15 Transmission (S_{21} magnitude and phase) of the tunable phase shifter

V. CONCLUSIONS

A left-handed metamaterial transmission-line with a reconfigurable band-pass characteristics is presented. This is accomplished by loading the traditional left-handed line with an additional

lumped shunt capacitor. The controllable shunt capacitor loading can be used to tune the band-pass and band-stop responses of the metamaterial. A detailed dispersion analysis was conducted to study the effcet of shunt capacitance on the fundamental harmonic band of the periodic structure and its associated stop bands. General design procedures were outlined for the metamaterial line with arbitrary phase shift, impedence, and band-pass/band-stop characteristics. These developed design equations were utilized to synthesize an equal split compact reconfigurable wilkinson power divider in the range of 0.72 GHz to 0.88 GHz and a tunable phase shifter with a dynamic phase range of 100 degrees at the center frequency of 505 MHz. An overall twleve-times size-reduction as compared to the conventional power divider was achieved. The size of the phase shifter is about 1/20 times the center operating wavelength. The limit on the tunable range was imposed by the varactor type available at the time of the design. The tunable range can be increased by selecting a different varactor with a wider range or by using a combination of varactors. The shunt-capacitor loaded left-handed lines are suitable for devices that require band-pass response, harmonic suppression, and high band-rejection of adjacent and spirious frequencies.

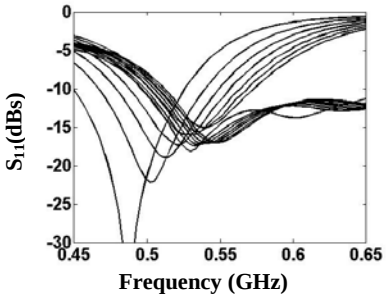

Fig. 16 The reflection (S_{11}) coefficient of the tunable phase shifter.

ACKNOWLEGGEMENT

The authors would like to acknowledge the assistance and the financial support provided by the Research Center at the College of Engineering at King Saud University for this project under grant number 7/430.

REFERENCES

[1] V.G. Veselego , "The Electrodynamics of Substanceswith Simultaneously Negative Values of ε and μ", *Soviet Physics Uspekhi*, Vol. 10, no. 4, pp. 509-514, Jan.-Feb.1968.

[2] R. A. Shelby, D. R. Smith, S. Schultz, "Experimental Verification of a Negative Index of Refraction," *Science*, vol. 292, pp. 77-79, April 2001.

[3] G.V. Eleftheriades and K.G. Balmain, Negative Refraction Metamaterials: Fundamental Principles and Applications, Toronto: John Wiley and Sons, 1st edition, 2005.

[4] C. Caloz, and T. Itoh, Electromagnetic Metamaterials: Transmission Line Theory and Microwave Applications, John Wiley & sons, Inc., 2006.

[5] S. A. Ramakrishna, "Physics of negative refractive index materials", Reports on Progress in Physics, vol. 68, no.2, February, 2005.

[6] A. K. Iyer, G. V. Eleftheriades, "Negative Refractive Index metamaterials supporting 2-D waves," IEEE MTT-S International Microwave Symposium Digest (Seattle, WA), vol. 2, pp. 1067-1070, June 2-7, 2002.

[7] C. Luo, S. Johnson, J. D. Joannopoulos, and J.B. Pendry, "All-angle negative refraction without negative effective index", Physical Review B, vol. 65, no. 13, pp. 2011041- 2011044, May, 2002.

[8] G.V. Eleftheriades, O. Siddiqui and A.K. Iyer, "Transmission line models for negative refractive index media and associated implementations without excess resonators." IEEE Microwave and Wireless Components Letters, vol. 13, no. 2, pp. 51-53, Feb. 2003.

[9] A. Grbic and G.V. Eleftheriades, "Overcoming the diffraction limit with a planar left-handed transmission-line lens." Phys. Rev. Lett., vol. 92, no. 11,pp. 117403 , March 19, 2004

[10] A .K. Iyer and G. V. Eleftheriades, "Mechanisms of sub-diffraction free-space imaging using a transmission-line metamaterial superlens: An experimental verification," Applied Physics Letters, 92, 131105, March 2008.

[11] G.V. Eleftheriades , "Enabling RF/Microwave Devices Using Negative-Refractive-Index Transmission-Line Metamaterials,", Radio Science URSI Bulletin, , no. 312, pp. 57-69 , March, 2005

[12] M.A. Antoniades and G.V. Eleftheriades, "Compact, Linear, Lead/Lag Metamaterial Phase Shifters for Broadband Applications," IEEE Antennas and Wireless Propagation Letters, vol. 2, issue 7, pp. 103-106, July 2003.

[13] C. Caloz, A. Sanada and T. Itoh, "A novel composite right-/left-handed coupled-line directional coupler with arbitrary coupling level and broad bandwidth" IEEE Transactions on Microwave Theory and Techniques, vol. 52, no. 3, pp. 980-992, March 2004.

[14] M. Antoniades and G.V. Eleftheriades, "A broadband Wilkinson balun using microstrip metamaterial lines," IEEE Antennas and Wireless Propagation Letters, , vol. 4, pp. 209-212, 2005.

[15] L. Sungjoon , C. Caloz, and T. Itoh, "Metamaterial-based electronically controlled transmission-line structure as a novel leaky-wave antenna with tunable radiation angle and beamwidth," IEEE Transactions on Microwave Theory and Techniques, vol. 52, no. 12, pp. 2678-2690, December 2004.

[16] H. Kim, A. Kozyrev, T. A. Karbassi, and D. Weide, "Linear Tunable Phase Shifter Using a Left-Handed Transmission Line", IEEE Microwave and Wireless Components Letters, Vol. 15, No. 5, pp. 366 – 368, May. 2005.

[17] O. Siddiqui, M. Mojahedi, and G.V. Eleftheriades, "Periodically loaded transmission line with effective negative refractive index and negative group velocity," IEEE Trans. on Antennas and Propagation, vol. 51, no. 10, 2619-2625, Oct. 2003.

[18] L. I-Hsiang M. DeVincentis, C. Caloz, and T. Itoh, "Arbitrary dual-band components using composite right/left-handed transmission line", IEEE Transactions on Microwave Theory and Techniques, vol. 52, no. 4, pp. 1142-1149, April 2004.

[19] Jun Hu, Jiang Xiong, Ti Ling, Yongzhuo Zou, "Design of a novel Wilkinson power splitter based on the left-handed transmission line", Microwave and Optical Technology Letters, Vol. 49, Issue 12, pp. 2975 – 2977, Sept. 2007.

[20] A.S. Mohra, "Compact dual band Wilkinson power divider", Microwave and Optical Technology Letters, Vol. 50, No. 6, pp. 1678 – 1682, June 2008.

[21] L. Wu, H. Yilmaz, T. Bitzer, and A. Berroth, "A Dual-Frequency Wilkinson Power Divider for a frequency and its first harmonic", IEEE Microwave and Wireless Components Letters, Vol. 15, No. 2, pp. 107 – 109, Feb. 2006.